IOP PUBLISHING JOURNAL OF MICROMECHANICS AND MICROENGINEERING

J. Micromech. Microeng. **18** (2008) 057001 (8pp) doi:10.1088/0960-1317/18/5/057001

NOTE

Design and fabrication of a high sensitivity focal plane array for uncooled IR imaging

Xiaomei Yu[1], Yuliang Yi[1], Shenglin Ma[1], Ming Liu[2], Xiaohua Liu[2], Liquan Dong[2] and Yuejin Zhao[2]

[1] National Key Laboratory of Nano/Micro Fabrication Technology, Institute of Microelectronics, Peking University, 100871 Beijing, People's Republic of China
[2] Department of Photo-Electronic Engineering, Beijing Institute of Technology, Beijing, 100081, People's Republic of China

E-mail: yuxm@ime.pku.edu.cn

Received 2 November 2007, in final form 1 February 2008
Published 25 March 2008
Online at stacks.iop.org/JMM/18/057001

Abstract
This note reports on the development of a novel cantilever-based focal plane array (FPA) for uncooled infrared (IR) imaging. The FPA of 160 × 120 pixels consisted of a 1 μm thick low stress SiN_x structure layer, a thin gold reflection layer and a thick gold bimaterial layer. A bulk silicon process that includes silicon–glass anodic bonding and deep reactive ion etching techniques was developed selectively to remove the substrate silicon and form silicon frames for every FPA pixel. The thermomechanical sensitivity of the cantilever pixel was measured as 0.11 μm K^{-1}, the noise-equivalent temperature difference of the FPA was theoretically estimated to be below 60 mK and the response time was calculated to be 15 ms. An optical readout system was used to measure deflections of all cantilevers in the FPA simultaneously, and thermal images of the human body were captured in good time. One of the unique advantages of this honeycomb-like FPA is the selective removal of the silicon substrate, which could increase the IR absorption efficiency by 48% compared with that fabricated by a traditional surface sacrificial layer process.

(Some figures in this article are in colour only in the electronic version)

1. Introduction

The infrared (IR) radiation imager is of importance for a wide range of applications, including military and civil uses. IR imagers with a cooling system are not widely used owing to cost, weight and power. Current microbolometer imaging technologies are not able to reach the sensitivity and time constant requirement for high performance IR detections. Researches have recently developed a new type of IR imager based on bimaterial cantilever arrays whose bending can be directly detected by optical means [1–11]. This approach eliminates the need for cooling and complex electronic multiplexers, holding the potential to reduce IR imager cost and weight drastically. In addition, the dominant thermal vibration noise enables the noise-equivalent temperature difference (NETD) to approach as low as 9 mK [6], which will offer a high detection sensitivity for the low-cost and low-power imaging system.

Considerable progress to reduce NETD and time constant has been made in recent years, and great achievements were obtained by some research groups [6–11]. In 2006, Grbovic *et al* of the Oak Ridge National Laboratory (Tennessee) reported a higher resolution array of 256 × 256 pixels [7, 8]. IR images of room temperature objects were obtained by use of these focal plane arrays (FPAs) with a response time of less than 15 ms and a NETD of ~500 mK. Agiltron Inc. produced a 280 × 240 photomechanical IR sensor with an optical readout for both mid-wavelength IR and long-wavelength IR imaging at a speed of up to 1000 frames per second [9]. Results on the detection of rapid occurrence events, such as gunfire and rocket travel, were reported. Hunter *et al* reported the development of small-pixel pitch IR FPAs that were based

Table 1. Thermophysical properties of SiN_x and gold.

Material	Density (10^3 kg m^{-3})	Young's module (GN m^{-2})	Thermal cond. (W m^{-1} K^{-1})	Expansion coeff. (10^{-6} K^{-1})	Heat capacity (J kg^{-1} K^{-1})
SiN_x	2.40	180	5.5 ± 0.5	0.8	691
Gold	19.30	73	296	14.2	129

on a capacitively read bimaterial microcantilever technology [10]. They modelled the performance of the innovative sensor structures, and indicated that NETDs were in the 1.0 K range and the thermal time constants were in the 5–10 ms range.

Cantilever-based IR imaging devices demonstrated to date are less sensitive than the theoretical predictions. There are many ways to improve the sensitivity including optimizing the design and improving the processes and readout system. For the FPA fabricated with a surface sacrificial layer process, cantilevers were anchored to a silicon substrate with a 2–3 μm spacing between them. The IR flux must transmit through the silicon substrate and the air layer before it reaches the cantilever pixels. Part of the IR radiation energy is therefore lost owing to the reflections and absorptions caused by the silicon substrate. In this note we report a novel honeycomb-like FPA with the substrate silicon selectively removed, and our experimental results show that this design is a very effective method in increasing the IR absorption efficiency and improving the IR imaging quality.

2. FPA design

2.1. Cantilever materials

The materials chosen to form the FPA structure should meet the following requirements: the IR-absorbing material must absorb IR light in the range of 8–14 μm, the reflecting material must be a good reflector in the visible spectrum to be suitable for optical readout, the thermal conductivity of the IR absorbing material must be low and the mismatch of expansion coefficients of the two materials should be as large as possible [2].

SiN_x material absorbs IR radiation in the range of 8–14 μm and is widely used as the structural material in fabricating a bimaterial cantilever FPA [1–11]. The thermal conductivity of SiN_x is very low, and SiN_x also shows a desirable large mismatch in the thermal expansion coefficient with metals. A low stress, low-pressure chemical vapour deposition (LPCVD) SiN_x film was therefore chosen to form the structure layer in this work. Gold shows much better anti-etching performances than aluminium in many etching solutions, so gold was used as the material for the visible light reflection and the bimaterial arm bending. The basic properties of SiN_x and gold are provided in table 1.

IR absorption spectra of the LPCVD SiN_x films with different thicknesses have been acquired by use of a Nicolet Magna 750 Fourier transform infrared spectrometer. The results are shown in figure 1. It can easily be seen from figure 1 that the IR absorption of SiN_x is proportional to the film thickness. The IR absorptivity can reach 0.97 for a 1.0 μm thick SiN_x film; hence, a 1 μm thick SiN_x film is used to fabricate the cantilever structure and serves as an IR absorber.

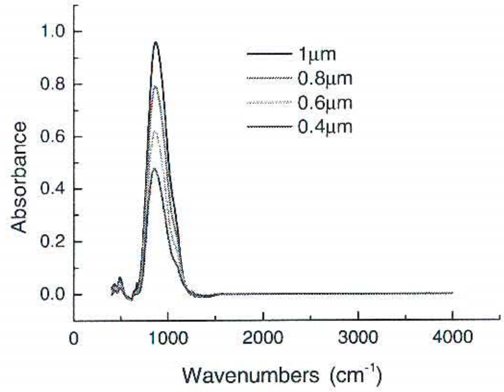

Figure 1. IR absorption spectra of LPCVD SiN_x films.

For a metal film with a thickness of more than 50 nm, the reflection coefficient to a visible light approaches 100%. In order to decrease the surface roughness and the reflector bending, a 50 nm gold film is deposited on the surface of the SiN_x absorber and serves as a reflecting mirror for the optical readout.

2.2. Cantilever design

An FPA of 160 × 120 cantilever pixels with a pinch of 146 μm × 110 μm was designed in this work, and a schematic diagram of a top view of the cantilever pixel is shown in figure 2(*a*). The cantilever, with a low stress LPCVD SiN_x film as the main structure layer, incorporates an IR absorber/reflector, two bimaterial arms and two thermal isolation arms. Gold films with different thicknesses were deposited on the surface of the IR absorber and the bimaterial arms. The absorber/reflector (80 μm × 60 μm) both absorbs the incident IR radiation with the SiN_x layer and reflects the visible light with the gold mirror. The folded bimaterial arms (80 μm × 4 μm each) will induce the thermal bending of the cantilever owing to the bimaterial effect and the isolation arms (80 μm × 4 μm each) provide thermal isolation of the cantilever structure from the substrate.

Figure 2(*b*) shows the schematic diagram of a cross-sectional view of the cantilever pixel. In our design the cantilever is attached mechanically to a silicon frame through the two cantilever arms, and the substrate silicon at which the cantilevers are located is selectively etched away. The side with the gold layers deposited is defined as the front side, whereas the other side is the back-side. During the imaging, IR flux radiates onto the cantilever pixels directly from the back-side, and the bimaterial cantilevers will undergo a downward bending owing to the dissimilar thermal expansion coefficients of SiN_x and gold. These bending are then read out with the reflecting mirrors by an optical readout system.

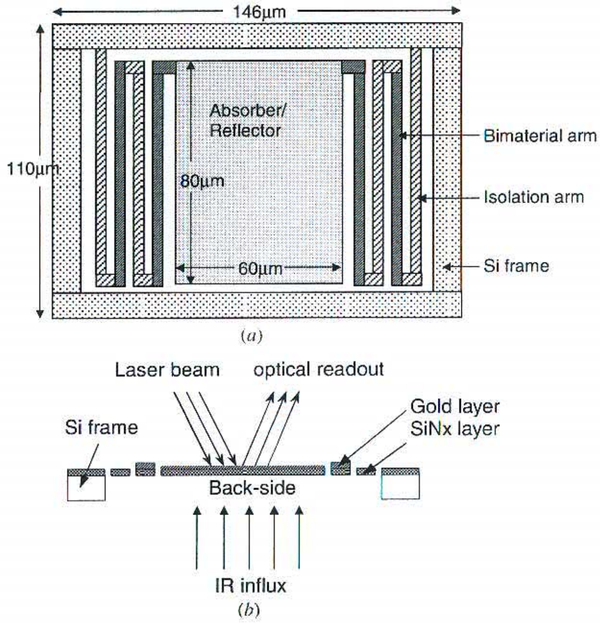

Figure 2. (*a*) Schematic diagram of the top view of a cantilever pixel. (*b*) Schematic diagram of the cross-sectional view of a cantilever pixel.

2.3. IR absorptivity

According to geometrical optics, the reflection coefficient R at the interface of two media is given by [12]

$$R = \left(\frac{N_1 - N_2}{N_1 + N_2}\right)^2, \qquad (1)$$

where N_1 and N_2 are the complex indices of refraction of two materials, respectively, and can be expressed as $n - \mathrm{i}k$, where n is the refractive index and k is the extinction coefficient. When the incident angle of light is near zero, k is several orders of magnitude smaller than n and can be ignored during the calculations. If both the reflection and transmission are considered, the total energy lost through the medium can then be calculated from [11]

$$R + R(1-R)^2 + R^3(1-R)^2 + \cdots. \qquad (2)$$

Suppose the initial incident IR energy is 1; the IR absorptivity can then be expressed as [11]

$$1 - R + R(1-R)^2 + R^3(1-R)^2 + \cdots. \qquad (3)$$

For the FPAs fabricated with a surface sacrificial layer process, all the cantilevers are fixed to a common substrate by anchors (figure 3). During imaging, the incident IR flux must first transmit through the silicon substrate and the air layer between the cantilever and the substrate before it reaches the IR absorber. Given the reflection and absorption through the silicon substrate, the IR absorptivity is calculated to be 0.54 in equations (1) and (3) for this type of FPA; n_{Si} and n_{air} are 3.4 and 1.0 during the calculation respectively.

For the FPA proposed in this work, IR energy losses through the silicon substrate are avoided by its selective removal. Given the reflection from the cantilever back-side, the IR absorptivity of the pixel is calculated to be 0.8 with

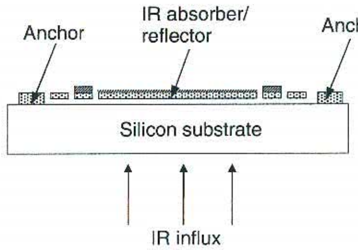

Figure 3. Cross-sectional view of a pixel structure fabricated with a surface sacrificial layer process.

$n_{\mathrm{SiN}x}$ of 2.0. This means that about 80% of the incident IR flux will radiate onto the SiN_x absorber and the IR absorption efficiency of this novel FPA is increased by 48% compared with that fabricated by the surface sacrificial layer process.

2.4. Thermomechanical sensitivity

The thermomechanical sensitivity S_{T} of a cantilever can be found to be [2]

$$S_{\mathrm{T}} = \frac{\delta}{\Delta T_{\mathrm{c}}} = 3(\alpha_{\mathrm{Al}} - \alpha_{\mathrm{SiN}x})\left(\frac{n+1}{K}\right)\left(\frac{L_m^2}{h_{\mathrm{SiN}x}}\right), \qquad (4)$$

where δ is the deflection of the cantilever at $x = L_m$, L_m is the length of the bimaterial arm, α is the thermal expansion coefficient of two materials, $n = h_{\mathrm{Gold}}/h_{\mathrm{SiN}x}$ is the ratio of the thickness of gold and SiN_x and $K = 4 + 6n + 4n^2 + \phi n^3 + 1/\phi n$ is the structure parameter where $\phi = E_{\mathrm{Gold}}/E_{\mathrm{SiN}x}$ is the ratio of the elastic modulus of gold and SiN_x. Given the thermophysical properties of SiN_x and gold in table 1 and the geometrical parameters in section 2.2, the thermomechanical sensitivity of the cantilever is calculated to be 0.11 μm K^{-1}.

ANSYS finite element software was used to model the thermomechanical properties of the cantilever so as to determine the gold layer thickness on the bimaterial arms. The simulated relation of the thickness ratio of two materials to the thermomechanical sensitivities is plotted in figure 4. During the simulations, the heat transfer was ignored for simplification and the thermophysical parameters of SiN_x and gold in table 1 were used. It could be seen that when the thickness ratio is around 0.5, the cantilever shows the biggest S_{T}. Therefore, a 0.5 μm thick gold film was applied as the second bimaterial layer in the following process.

The vertical deformations of the fabricated cantilever versus the temperature change are measured by a profile meter, and figures 5(*a*) and (*b*) are the measured results of the cantilever configurations at the temperatures of 19 °C and 36 °C, respectively. S_{T} is then calculated from the vertical position at the cantilever end to be 0.11 μm K^{-1}, which is equal to the theoretical result.

3. Fabrication

The FPA fabrication, including four photolithographic steps, is illustrated in figure 6. The fabrication started from a double-sided polished silicon wafer with a thickness of 300 μm. The detailed micromachining steps are as follows. (a) A deposition

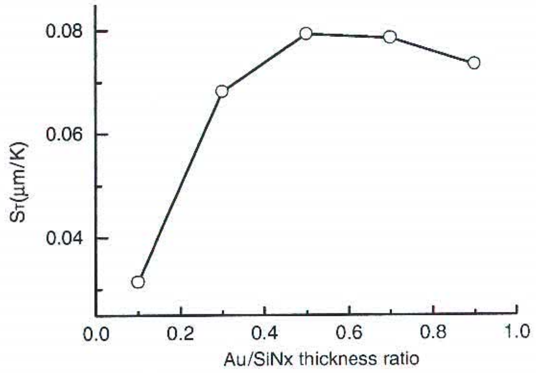

Figure 4. Simulated relation of the thickness ratio to thermomechanical sensitivities.

of a 200 nm thick SiO_2 film to form the etching buffer layer between the structure layer and the substrate, and a deposition of low stress LPCVD silicon nitride film of 1.0 μm thickness. (b) A 0.5 μm thick gold film was sputtered and patterned to form the bimaterial arms with a wet etching technique. (c) In order to decrease the bending and the surface roughness of the cantilever reflector, only a 50 nm gold film was sputtered on the SiN_x absorber and patterned with a lift-off technique as the reflecting mirror. (d) The SiN_x cantilever structure was patterned with the reactive ion etching (RIE) technique. (e) A glass wafer was patterned and etched in an HF solution to form a 50 μm deep cavity, and the length and width of the cavity are the same as the FPA. (f) The glass and silicon wafers were anodic bonded together. Here, the glass wafer was used as a supporting wafer to avoid the thin FPA structure from breaking. (g) Thinning down the silicon wafer to 100 μm from the other side in the KOH solution, to increase the etching uniformity and decrease the footing effect in the following inductively coupled plasmas' (ICPs) etching. (h) Double-side lithography was used to pattern the back-side silicon. Finally, the silicon substrate was anisotropically etched in an ICP system and the

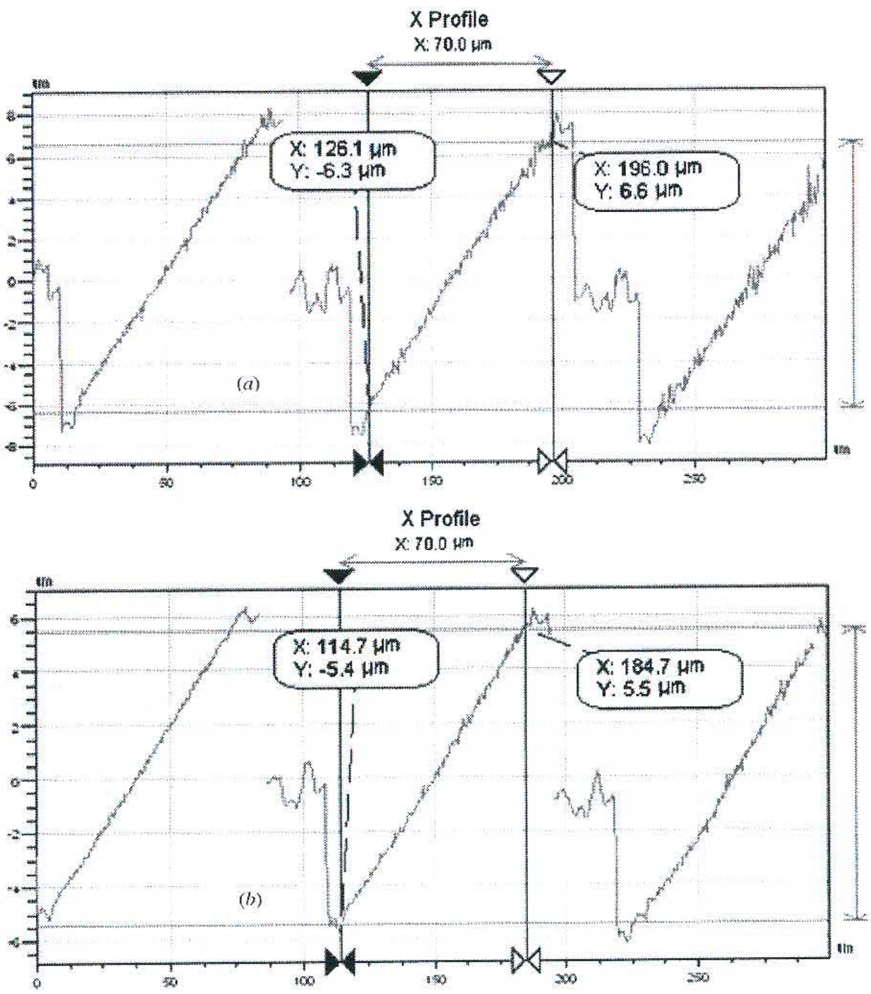

Figure 5. Vertical deformations of a cantilever measured by a profile meter at temperatures of 19 °C (*a*) and 36 °C (*b*), respectively.

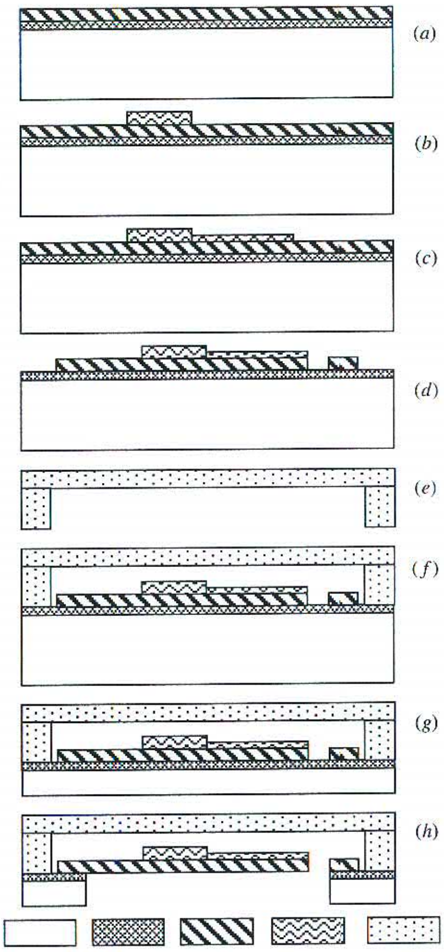

Figure 6. Fabrication process of the FPA: (*a*) 200 nm SiO2 film and 1 μm SiN_x film were deposited on a silicon substrate, (*b*) thick gold film (500 nm) for a bimaterial beam was sputtered and patterned, (*c*) thin gold film (50 nm) for a reflector was patterned by the lift-off technique, (*d*) SiN_x cantilever was patterned and etched in a RIE system, (*e*) 50 μm deep cavity was etched on a glass wafer, (*f*) silicon–glass anodic bonding, (*g*) silicon substrate down to 100 μm in a KOH solution, (*h*) double-sided lithography and anisotropy dry etching of Si and SiO_2.

SiO_2 buffer layer was removed in the RIE system. Figure 7 is a scanning electron microscope (SEM) photo of the FPA with an enlarged view of a cantilever pixel.

In this process, a deep reactive ion etching (DRIE) technique was used to selectively remove the substrate silicon at the area where the cantilevers are located and form a honeycomb-like silicon frame for each of the cantilever pixels. The IR reflection and the absorption through the silicon substrate could therefore be completely avoided. The main problem in this process is the pixel-to-pixel mechanical uniformity, which depends on the etching uniformity of the ICP system. By use of the SiO_2 buffer layer and the KOH thinning technique, the etching uniformity could be improved greatly although the etching uniformity of our ICP system is not in a good state. It was estimated that a pixel-to-pixel uniformity of better than ±5% was achieved on the whole FPA with a dimension of 1.4 mm × 1.8 mm.

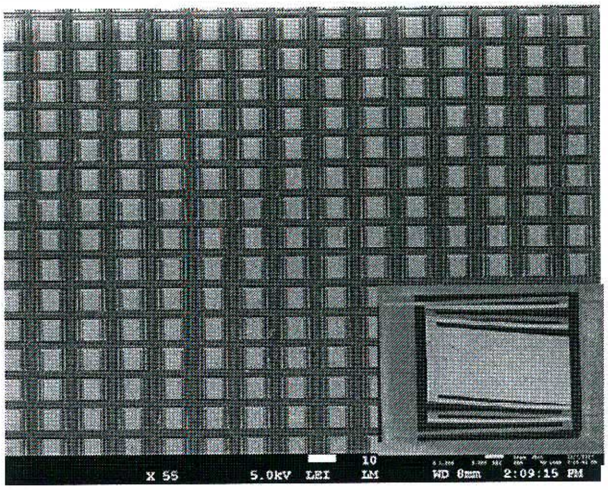

Figure 7. SEM photo of the FPA with an enlarged view of a cantilever pixel.

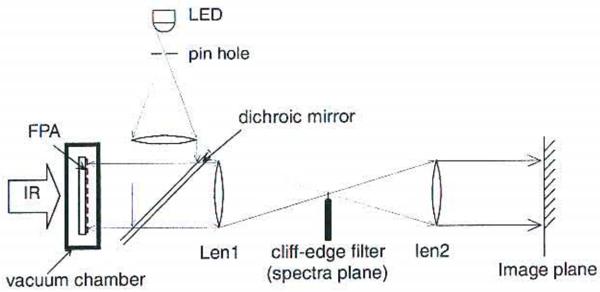

Figure 8. Schematical diagram of the optical readout system.

4. Imaging and analysis

4.1. IR imaging

The optical readout system for the IR imaging is schematically shown in figure 8, and a detailed description of the IR and visible light paths is shown in figure 2(*b*). The IR flux radiates onto the FPA through an IR lens, and the FPA is sealed in a vacuum chamber with a 10 mTorr pressure to prevent the dissipation of heat. An LED illuminates the mirrored photomechanical cantilever array with a collimating lens reflected from the gold mirrors. The reflected LED light passes through a transforming lens (lens 1) and synthesizes the spectra of the cantilever array on the rear focal plane of the lens. With a cliff-edge filter placed in the rear focal plane, which is defined as a spectra plane, the deflection of all pixels in the FPA is simultaneously measured and projected as a spatially varying visible light image onto an image plane. Thermal images of IR objects were captured to demonstrate the IR imaging capability of the FPA and the system. Figure 9 shows iron IR images at the detecting distances of 0.8 m, 1.1 m and

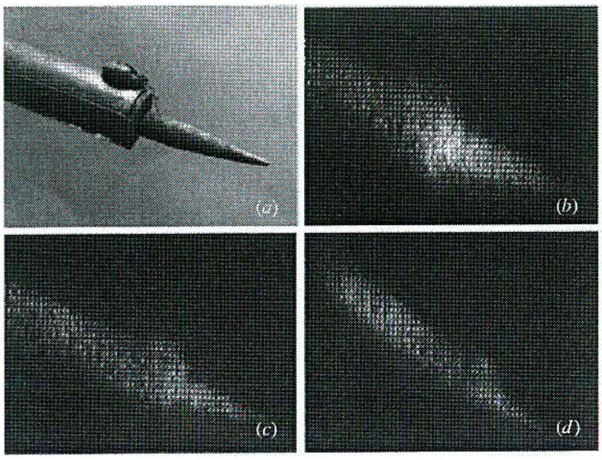

Figure 9. Iron (*a*) IR images at the detecting distances of 0.8 m (*b*), 1.1 m (*c*) and 1.4 m (*d*), respectively.

1.4 m, and figure 10 shows two thermal images of a person's hand and face respectively.

4.2. Noise analysis

NETD, defined as the scene temperature change that causes the signal to be equal to the noise of the system, is usually calculated to evaluate the performance of the detectors further. Several sources would introduce noises to the thermal detector regardless of readout methods. These include temperature fluctuation noise, background fluctuation noise and thermal-mechanical noise from thermally excited vibration of the cantilever. The optical readout system will introduce shot noise to the imaging system.

The temperature fluctuation noise is a random fluctuation in the temperature of the thermodynamic system, arising from the statistical nature of the heat interchange with its surroundings. Because the FPA is packaged in a vacuum, the main heat loss will be because of thermal conduction along the arms of the detector. Assuming that the radiative heat exchange between the detector and its surroundings is small enough compared with the conduction exchange, the temperature fluctuation NETD, $\mathrm{NETD_{tf}}$, can be written as [5, 6]

$$\mathrm{NETD_{tf}} = \frac{8F^2 T_\mathrm{D}\sqrt{k_\mathrm{B} B G}}{\eta\tau_0 A_\mathrm{D}(\mathrm{d}P/\mathrm{d}T)_{\lambda 1-\lambda 2}}, \qquad (5)$$

where F is the f number of the optics, T_D is the detector temperature, k_B is the Boltzmann constant (1.38×10^{-11} pJ K^{-1}), B is the noise bandwidth, τ_0 is the transmission efficiency of the optics, η is the IR absorptivity of the detector, A_D is the detector area and $(\mathrm{d}P/\mathrm{d}T)_{\lambda 1-\lambda 2}$ is the IR target power emission rate per unit area radiated by a blackbody at temperature T within the special band from $\lambda 1$ to $\lambda 2$. G is the total thermal conductance of two arms, which can be expressed as [2]

$$G = A_\mathrm{arm} k / L_\mathrm{arm}, \qquad (6)$$

where A_arm is the cross-sectional area of the arm, k is the thermal conductivity of the arm material and L_arm is the total length of the arm. $\mathrm{NETD_{tf}}$ can be calculated as 5.1 mK; the values used for the calculation were $F = 1$, $B = 30$ Hz, $T_\mathrm{D} = 300$ K, $A_\mathrm{D} = 4800\ \mu\mathrm{m}^2$, $G = 1.4 \times 10^{-7}$ W K^{-1}, $\eta = 0.8$, $\tau_0 = 0.5$ [6], $(\mathrm{d}P/\mathrm{d}T)_{8-14\ \mu\mathrm{m}} = 2.62$ pW $(\mu\mathrm{m})^{-2}$ K [6].

The background fluctuation noise ($\mathrm{NETD_{bf}}$) is the radiative heat exchange between the thermal detector and its surroundings, which can be written as [5, 6]

$$\mathrm{NETD_{bf}} = \frac{8F^2\sqrt{2k_\mathrm{B}\sigma B\left(T_\mathrm{D}^5 + T_\mathrm{B}^5\right)}}{\eta\tau_0 (A_\mathrm{D})^{1/2}(\mathrm{d}P/\mathrm{d}T)_{\lambda 1-\lambda 2}}, \qquad (7)$$

where σ is the Stefan–Boltzmann constant (5.67×10^{-8} pW $(\mu\mathrm{m})^{-2}$ K^4) and T_B is the background temperature (300 K). It can be calculated that $\mathrm{NETD_{bf}}$ is 1.7 mK.

When the device is in thermal equilibrium with its surroundings, there is a continuous exchange of the mechanical energy accumulated in the device with the thermal energy of the surroundings, which gives rise to a spontaneous vibration. This would cause a vibration noise in the detector. Because the IR detector needs to be packaged in a vacuum environment in order to minimize the convection losses, as described earlier, a model based on the internal friction process is used to describe this thermal-mechanical noise, and $\mathrm{NETD_{tm}}$ can be written as [6]

$$\mathrm{NETD_{tm}} = \frac{8F^2}{\eta\tau_0 S_\mathrm{T}(\mathrm{d}P/DT)_{\lambda 1-\lambda 2}}\sqrt{\frac{k_\mathrm{B} B T_\mathrm{D}}{k_\mathrm{s} Q\omega}}, \qquad (8)$$

Figure 10. Thermal images of a person's hand and face.

where S_T is the displacement sensitivity, which is measured at $0.11\ \mu m\ K^{-1}$, Q is the quality factor of the system, ω is equal to 15.0 Hz as the centre frequency of a 30 Hz bandwidth and k_s is the spring constant of the structure. For the structure, a model analysis shows that $k_s = 0.26\ \mu N\ \mu m^{-1}$ and $Q = 3000$ can be obtained in a vacuum environment. $NETD_{tm}$ can then be calculated to be 60 mK.

Since these noise sources are probabilistic and assumed to be statistically uncorrelated, the total noise in the FPA is equal to the square root of the sum of the squares of the individual noise sources [6]:

$$NETD_{total} = \sqrt{DETD_{tf}^2 + NETD_{bf}^2 + NETD_{tm}^2}. \quad (9)$$

The above analysis shows the potential to achieve a value of $NETD_{total}$ below 60 mK.

It can be seen from the above equations that all the NETDs are inversely proportional to the IR absorptivity η. For the FPAs fabricated by the sacrificial layer processes, 46% of the IR radiation will be reflected and absorbed by the silicon substrate, whereas only 20% of the IR radiation is reflected from the FPA fabricated in this work. If other IR energy losses are not considered, the $NETD_{total}$ of this FPA is decreased by 48% compared with that fabricated with the surface sacrificial layer process.

4.3. Time constant

The response time of a cantilever pixel depends on its dimension and material properties, and is expressed as [2]

$$\tau = C_{th}/G, \quad (10)$$

where C_{th} is the pixel thermal capacitance and G is the thermal conductance. Along with the pixel dimension designed above and the material properties from table 1, τ is calculated to be 15 ms under a 10 mTorr pressure. For a photomechanical imaging pixel, the rising or falling time of the cantilever pixel in response to a short pulse is significantly shorter than its inherent thermal time constant [9]. Besides, the heat source input into the photomechanical pixel is only the incident IR radiation and Joule heating from the electrical readout is eliminated, resulting in an enhanced responsivity. Thus, the optical readout photomechanical imager may be operated with a much higher speed than the calculated results.

4.4. Reflector shape distortion and surface roughness

For the optical readout system shown in figure 8, the angular width of zero-order spectra on the spectra plane is

$$\frac{\lambda}{a}. \quad (11)$$

The angular detection resolution can be expressed as

$$\frac{\lambda}{2Na}; \quad (12)$$

here a is the reflector width, λ is the wavelength of the visible light and N is the grey-level resolution of a CCD. With the values of $a = 60\ \mu m$, $\lambda = 0.6\ \mu m$ and $N = 4096$ that is calculated from a 12 bit CCD, an angular detection resolution of 2×10^{-6} rad is thus obtained. The angular detection sensitivity is determined by the angular width of the zero-order spectra.

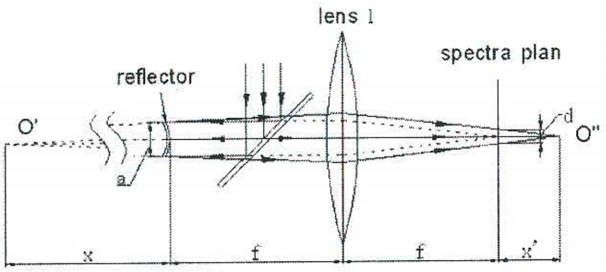

Figure 11. Schematical diagram of widening spectra caused by a convex reflector.

Since a cliff-edge filter was used to cut off the reflected spectra on the spectra plane in the optical readout system, changes in the reflected spectra direction will remarkably influence the angular width and therefore the detection sensitivity. Two main limitations in reflection mirrors will result in the widening on the spectra plane: one is the reflector surface roughness caused by a thicker film deposition and the other is the detector bending caused by the bimaterial effect.

The surface bending caused by the mismatch of two materials in a reflector will form a concave or a convex mirror. An instance of a convex mirror is shown in figure 11, and a concave mirror will work in a similar way. In figure 11, O′ is a virtual light source of the convex mirror, which is also a focal point of the convex mirror; O is an image of O′ imaged by lens 1, which is not on the spectra plane due to the widening spectra. An actual spectra width (d) on the spectra plane, which can be used to evaluate the widening effect of the convex reflector, can be expressed as

$$d = d_0 + \frac{\lambda f}{a}; \quad (13)$$

here d_0 is an ideal spectrum width. If only geometrical optics is considered and the mirror is flat, d is zero. Then the actual angular detection resolution is

$$\frac{d}{2Nf} = \frac{a}{2Nx} + \frac{\lambda}{2Na}; \quad (14)$$

here x is the focal length of the convex mirror. The actual spectra width should not be two times bigger than the ideal spectra width, $d \leqslant \frac{\lambda}{a} f$, so $x \geqslant \frac{a^2}{\lambda}$ can be obtained. With the geometrical dimension given above, the limit on x is calculated to be 6.0 mm. The chord height h of the convex mirror can be calculated from

$$h = 2x - \sqrt{4x^2 - \frac{a^2}{4}}. \quad (15)$$

h is calculated to be 38 nm by equation (15). This means that the chord height of the bended reflector has to be less than 38 nm in order to ensure that the IR image was effectively detected.

Scattering is the redirection of the incident radiation into a different propagation direction. A surface roughness of the reflection mirrors could produce a light scattering and widen the spectra width. The scattering spectra width in a particular direction should not be two times bigger than the width of zero-order spectra on the spectra plane, so as to be well filtered by the cliff-edge filter. When light radiates onto the surface of a medium, the scattering light intensity I_s in a solid angle of $\Omega - \Omega + \mathrm{d}\Omega$ can be expressed as [13]

$$I_s = 4k^4 \sin\theta_i \cdot \cos^2\theta_s \cdot Q \cdot W(p \cdot q)\,\mathrm{d}\Omega. \qquad (16)$$

Here θ_i is the incident angle of the light, θ_s is the scattering angle, k is the wave number $k = 2\pi\ \lambda^{-1}$, Q is the polarization factor and $W(p, q)$ is the power spectra density of a surface contour related to the surface roughness, which can be expressed with equation (17) by considering the reflector as an axis symmetrical structure [13]:

$$W(p) = \frac{1}{L}\frac{1}{2\pi}\left|\int_{-L/2}^{L/2} \mathrm{e}^{\mathrm{i}px} z(x)\,\mathrm{d}x\right|^2; \qquad (17)$$

here L is the correlation length, which is determined by the degree of the surface roughness. In order to decrease the light scattering from a surface protuberance, L should be as large as possible. It is estimated that more than 20% of the incident IR energy could be scattered if $\theta_i = 10°$, $\lambda = 0.6\ \mu$m, $L = 0.1\ \mu$m.

The shape distortion and the surface roughness of the reflector have a serious influence on the IR imaging quality. This is experimentally confirmed by a comparison of this work with our former work [14]. The main difference between the two is that a thicker metal film was used as the reflection mirror in the first work, and only a 55 °C detection temperature was achieved with that FPA.

5. Conclusions

We have explored the design, process and performance of a microcantilever array as an IR FPA and demonstrated that the images obtained with this FPA can be enhanced greatly. Silicon–glass anodic bonding and DRIE techniques were introduced to fabricate the silicon frames-supported FPA, and a pixel-to-pixel uniformity of better than ±5% can be achieved. The IR absorptivity of the FPA is calculated to be about 80% and increased by 48% compared with that fabricated by the surface sacrificial layer process. Experimental and calculated results show that the fabricated FPA has a 0.11 μm K^{-1} thermomechanical sensitivity, a 15 ms time constant and a less than 60 mK NETD. Finally, the influences of the reflector shape distortion and the mirror surface roughness on the imaging quality are analysed.

Acknowledgments

This work is supported by the Hi-Tech Research and Development program of China (founded no. 2006AA04Z336) and National Natural Science Foundation of China (founded nos. 50730009 and 60776055).

References

[1] Tribolet P, Chorier P, Manissadjian A, Costa P and Chatard J 2000 High performance infrared detectors at Sofradir *Proc. SPIE* **4028** 54

[2] Zhao Y, Mao M, Horowitz R, Majumdar A, Varesi J, Norton P and Kitching J 2002 Optomechanical uncooled infrared imaging system: design, microfabrication, and performance *J. Microelectromech. Syst.* **11** 136–46

[3] Mao M, Perazzo T, Kwon O and Majumdar A 1999 Direct-view uncooled micro-optomechanical infrared camera *Proc 12th IEEE Int. Conf. MEMS (17–21 January)* pp 100–5

[4] Choi J, Yamaguchi J, Morales S, Horowitz R, Zhao Y and Majumdar A 2004 Design and control of a thermal stabilizing system for a MEMS optomechanical uncooled infrared imaging camera *Sensors Actuators* A **104** 132–42

[5] Ishizuya T, Suzuki J, Akagawa K and Kazama T 2002 160 × 120 pixels optically readable bimaterial infrared detector *Proc. 15th IEEE Int. Conf., MEMS (20–24 January)* pp 578–81

[6] Datskos P G 2004 Performance of uncooled microcantilever thermal detectors *Rev. Sci. Instrum.* **75** 1134–48

[7] Grbovic D, Lavrik N V and Datskos P G 2006 Uncooled infrared imaging using bimaterial microcantilever arrays *Appl. Phys. Lett.* **89** 073118

[8] Lavrik N, Archibald R, Grbovic D, Rajic S and Datskos P 2007 Uncooled MEMS IR imagers with optical readout and image processing *Proc. SPIE* **6542** 65421E

[9] Salerno J P 2007 High frame rate imaging using uncooled optical readout photomechanical IR sensor *Proc. SPIE* **6206** 65421D

[10] Hunter S R, Mgoldrer G S, Jiang L and Simelgor G 2007 High sensitivity uncooled microcantilever infrared imaging arrays (invited paper) *Proc. SPIE* **6542** 65421F

[11] Li C, Jiao B, Shi S, Chen D, Ye T, Zhang Q, Guo Z, Dong F and Miao Z 2006 Novel uncooled substrate-free optical-readable infrared detector: design, fabrication and performance *Meas. Sci. Technol.* **17** 1981–6

[12] Mu G and Zhan Y 1981 *Optics* (China: People's Education)

[13] Tian L 2003 Wavelength roughness and light scattering *Optoelectron. Technol. Inf.* **16** 37–9

[14] Wang X, Ma S, Yu X, Liu M, Liu X and Zhao Y 2007 IR imaging using a cantilever-based focal plane array fabricated by deep reactive ion etching technique *Appl. Phys. Lett.* **91** 054109